Journal of Alloys and Compounds 735 (2018) 430–440

Contents lists available at ScienceDirect

Journal of Alloys and Compounds

journal homepage: http://www.elsevier.com/locate/jalcom

Effect of vapor deposition in shrouded plasma spraying on morphology and wettability of the metallic Ni20Cr coating surface

Jie Li, Cheng-Xin Li*, Guan-Jun Yang, Chang-Jiu Li

State Key Laboratory for Mechanical Behavior of Materials, School of Materials Science and Engineering, Xi'an Jiaotong University, Xi'an, Shaanxi 710049, PR China

ARTICLE INFO

Article history:
Received 17 May 2017
Received in revised form
1 November 2017
Accepted 10 November 2017
Available online 13 November 2017

Keywords:
Shrouded plasma spraying
Vapor deposition
Nanostructure
Wettability transition
Super-hydrophobicity
Hydrocarbons

ABSTRACT

A Ni20Cr coating surface with a micro-nano hierarchical structure was successfully prepared by shrouded plasma spraying method in the present study. By adjusting the spraying parameters to control the heating degree of the powder particles and using a designed shield deposition method, we confirmed that the nanostructures were the products of vapor deposition by vaporization of the material during the spraying. In addition, an interesting phenomenon was found that, without any additional chemical modification, the surface with micro-nano structures underwent a wettability transition from super-hydrophilicity to super-hydrophobicity during the storage in air. The results show that the selective spontaneous adsorption of the nanostructures can effectively reduce the surface free energy. The nanostructures deposited on the top of the surface made the surface form a unique hierarchical structure, which can effectively reduce the contact area of the droplet with the surface. Nanostructures affected the wettability of the coating surface both in the chemical composition and the structural aspects, which demonstrated that they were the key to obtaining super-hydrophobic property on the coating surface.

1. Introduction

Atmospheric plasma spraying is an extensively used coating preparation method currently. With its high deposition rate and relatively low costs, the method has good application prospects, especially in the preparation of functional metals and alloy coatings [1]. The coating preparation in this process is based on the feedstock being heated in a high temperature plasma jet to a molten or partially molten state, impacting on the substrate surface at high speed and then flattening and solidification [2]. Surface morphology can significantly affect the properties of the coating surface, so controlling the surface microstructures by adjusting the spraying parameters is important for regulating its performance. The solid powder particles with micron size typically larger than 5 μm are commonly used as feedstock, the typical morphology of the coating surface usually presents micron convex structures, accompanied by a small amount of sub-micron splashes. According to the current researches, the presence of nanostructures was rarely observed on the coating surface prepared by atmospheric plasma spraying [3–6].

Wettability is one of the most important properties of solid surface, which is influenced by geometrical structure and chemical composition of the surface [7,8]. Generally, when the contact angle of a droplet on the surface is lower than 90°, the surface is hydrophilic. On the contrary, when the contact angle is greater than 90°, the surface is hydrophobic [9]. Among them, super-hydrophobic surface with contact angle greater than 150° and sliding angle lower than 10° has attracted much attention of researchers because of its potential application prospects in anti-fouling, anti-corrosion and so on [10]. However, there are very few reports focus on the study of coating surface wettability in the field of atmospheric plasma spraying [5]. As a simple and fast coating preparation method, the research on the coating surface wettability especially the super-hydrophobic property can not only develop a new application for the plasma spraying method, but also provide an effective and feasible way for the preparation of super-hydrophobic surface.

Metals and alloys are the widely used engineering materials which have a high surface free energy [11]. When these hydrophilic materials are used to prepare super-hydrophobic surfaces, it is necessary to reduce the surface free energy by chemical modification. However, the high cost and the complex process of the

* Corresponding author.
E-mail addresses: crystallijie@163.com (J. Li), licx@mail.xjtu.edu.cn (C.-X. Li), ygj@mail.xjtu.edu.cn (G.-J. Yang), licj@mail.xjtu.edu.cn (C.-J. Li).

https://doi.org/10.1016/j.jallcom.2017.11.135
0925-8388/

modification process made it highly desirable for researchers to find methods without chemical modification [4]. The preparation of super-hydrophobic surfaces directly through hydrophilic materials is an innovative research with full of challenges. In recent years, a small number of related researches have been emerged. However, the methods were diverse and the authors held different views. The research in this area was not yet mature. In some studies, the authors believed that the suitable rough structure on the surface was the key to directly achieving super-hydrophobicity [12–14]. In other researchers' point of view, the surface with a rough structure prepared by hydrophilic materials can achieve super-hydrophobicity by reducing the surface free energy through spontaneous adsorption or reaction with the substances from the surrounding air, such as oxygen, carbon dioxide and hydrocarbons [5,15–18].

In the present work, a micro-nano hierarchical Ni20Cr coating surface was prepared by shrouded plasma spraying method. Shrouded plasma spraying is one of atmospheric plasma spraying method, which is characterized by the installation of a gas shroud in front of the nozzle during the spraying. The nanostructures were successfully deposited on the surface by this method. Without any additional chemical modification, the coating surface can obtain super-hydrophobic performance after storage in air for a period of time. We achieved the purpose of using a simple one-step method for preparing super-hydrophobic surface. However, the formation process and control factors of the nanostructures in plasma spraying remained unclear, and the reasons for the surface wettability transition were yet to be identified. Therefore, there are two objectives of the present work. One is to investigate the formation mechanism of the nanostructures on the coating surface. Another is to clarify the reason of spontaneous acquisition of super-hydrophobic performance on the coating surface. This work intended to provide a theoretical basis for the one-step preparation of super-hydrophobic surfaces by atmospheric plasma spraying.

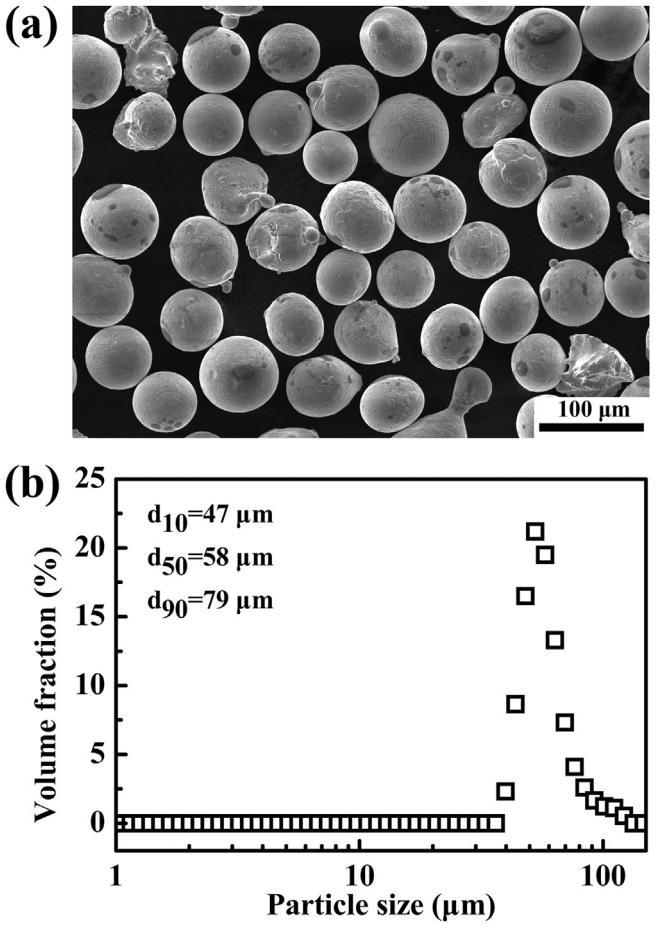

Fig. 1. Characterization of the feedstock Ni20Cr powder. (a) The typical morphology and (b) the particle size distribution.

2. Experimental

2.1. Materials

A commercially available Ni20Cr powder (PR2111, XianDao, China) mainly composed of spherical particles was used as feedstock. Typical morphology of the powder is shown in Fig. 1(a). The size distribution of the powder was measured by particle size analyzer (Toshima MFG Co., Ltd, Japan) as shown in Fig. 1(b). The powder had an essential lognormal distribution with characteristic particle sizes of 47 μm (d_{10}), 58 μm (d_{50}), and 79 μm (d_{90}). 304 stainless steel and copper plates with dimensions of Φ20 × 2 mm were used as substrates. Prior to spraying, the 304 stainless steel substrate was sandblasted and then ultrasonically cleaned with alcohol and acetone. For copper substrate, the surface was mirror polished, followed by ultrasonic cleaning with alcohol and acetone before deposition.

2.2. Coating preparation method

Shrouded plasma spraying (SPS) was used for coating deposition in this study. A plasma spraying system (GDP-80, Jiujiang, China) was employed to deposit coatings on the substrates. The plasma torch fixed on a six-axis robot was operated to generate an Ar-H_2 plasma jet. N_2 gas was used as a powder carrier gas. The powder was fed into the plasma jet using an internal powder injection. A gas shroud of argon attached in front of the plasma torch was utilized to minimize the oxidation of particles during in-flight process. The concentration of argon was 99.99%. The gas shroud has an inner diameter of 50 mm and a length of 110 mm. Internal Ar gas flow was employed to form a gas cone between the shroud wall and the plasma jet. The separation distance from the shroud exit to the substrate surface was set as 15 mm. Table 1 shows the detailed spraying parameters. The deposition process was performed in the atmospheric environment under room temperature. Three sets of parameters were used for the deposition and the effect of spraying power and hydrogen flow rate on the morphologies of coating surfaces was investigated, respectively. After spraying, the freshly prepared samples were stored in air in an ordinary plastic sample box.

2.3. Characterization methods

The morphologies of the feedstock powder and coating surfaces were characterized by field emission scanning electron microscopy (FESEM, MIRA3 LMH, TESCAN, Czech Republic). Further detailed structural information was characterized by transmission electron microscopy (TEM, Tecnai G2 F30, America) and the elemental analysis was performed using an energy dispersive X-ray spectroscopy (EDX) which was attached to the TEM equipment. X-ray photoelectron spectrometry (XPS, K-Alpha, Thermo Scientific, America) with a standard Al Kα radiation of 1486.68 eV was used to determine the valence states and the content of the elements present on the coating surface. The binding energy was calibrated using C 1s peak (284.6 eV). The contact angle (CA) and sliding angle (SA) of the water droplet on the coating surface were used to evaluate the wettability of the surface, detected by a contact angle

Table 1
Deposition conditions and parameters of shrouded plasma spraying.

Parameters	Unit	Value		
		SPS-1	SPS-2	SPS-3
Primary gas (Ar) flow rate	$L \cdot min^{-1}$	50		
Secondary gas (H_2) flow rate	$L \cdot min^{-1}$	6	3	6
Spraying power	kW	40	20	20
Carrier gas (N_2) flow rate	$L \cdot min^{-1}$	8		
Gun travelling speed	$mm \cdot s^{-1}$	50		
Spraying distance	mm	125		
Powder feeding rate	$g \cdot min^{-1}$	20		
Protective gas (Ar) flow rate	$L \cdot min^{-1}$	20		
Anode-nozzle internal diameter	mm	8		

instrument (JC2000C4, Shanghai Zhongchen Digital Technic Apparatus Co., Ltd., China). The volume of a freshly distilled water droplet used for the measurement was 5 μL. The static contact angle was measured using a typical sessile drop method by dropping a water droplet on the surface. While the sliding angle was measured by putting a water droplet on the horizontal surface and then tilting the surface until the droplet began to move. The inclination angle of the surface was considered as the sliding angle. At least 5 droplets were used to measure each sample at different locations. The chemical composition of the samples was investigated by a Fourier transform infrared spectroscopy (Vertex70, Bruker, Germany) with a resolution of 4 cm^{-1} and 64 scans. The substrate temperature was measured by a non-contact infrared thermometer (AR892+, Smart Sensor, China) during spraying.

3. Results and discussion

3.1. Surface morphology of the coatings

Fig. 2 shows the surface morphologies of Ni20Cr coating (SPS-1) under different magnification deposited by shrouded plasma spraying. As can be seen from Fig. 2(a), the surface presented a typical rough morphology of plasma sprayed coating consisted of splats and convex structures, which was formed by the random stacking of the molten or partially molten particles. However, it is worth noting that, unlike the conventional surface morphology deposited by atmospheric plasma spraying, the densely distributed nanostructures were found on the whole as-sprayed coating surface as shown in Fig. 2(b). Under a high magnification shown in Fig. 2(c–d), it can be seen that the nanostructures had fluff-like features, and the size of which was much smaller than that of the feedstock particles. The as-sprayed surface showed a unique micro-nano hierarchical structure.

When the spraying power was reduced to 20 kW and the hydrogen flow rate was reduced to 3 L/min during the deposition process, the nanostructures completely disappeared on the as-sprayed coating surface (SPS-2) as shown in Fig. 3(a, c). The surface was entirely consisted by micron-scale structures. On the basis of the process parameters of SPS-2, when the auxiliary gas flow rate of hydrogen was increased to 6 L/min, the fluffy nanostructures re-appeared on the whole prepared coating surface (SPS-3) especially on the convex positions, as can be seen in Fig. 3(b, d).

During the plasma spraying, both of the spraying power and the auxiliary gas flow rate of hydrogen are the important parameters

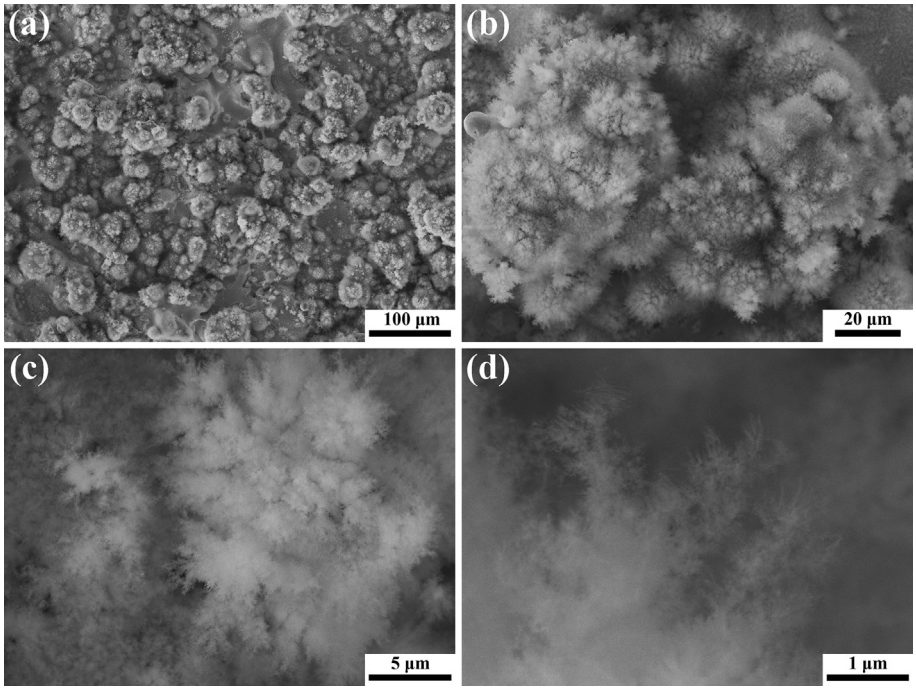

Fig. 2. Typical morphologies of Ni20Cr coating surface under different magnification deposited by shrouded plasma spraying using the parameter of SPS-1.

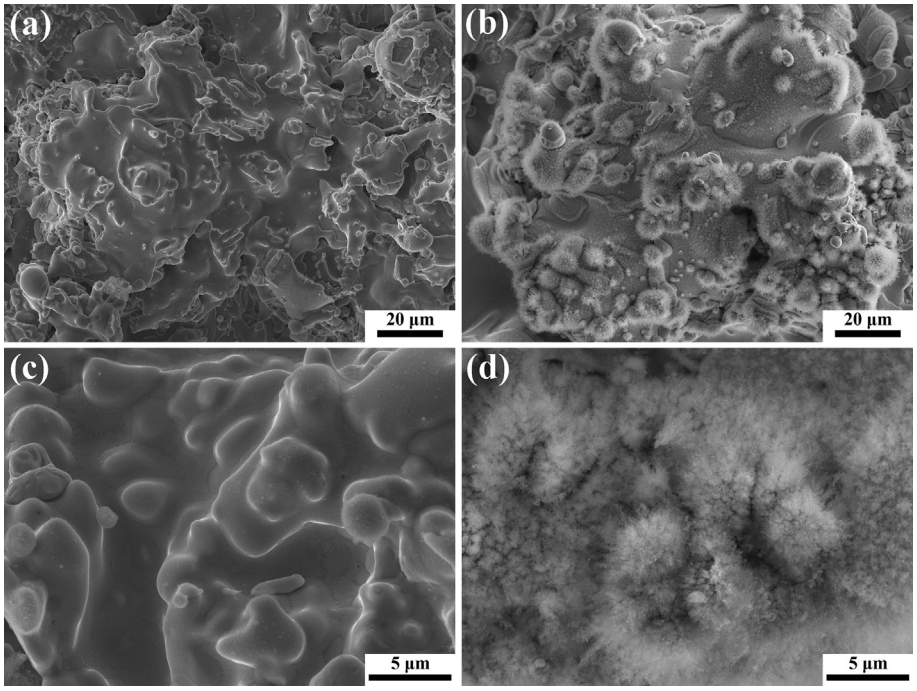

Fig. 3. Surface morphologies of the shrouded plasma sprayed coating surfaces deposited by different parameters. (a, c) Depositing with the hydrogen flow rate of 3 L/min and spraying power of 20 kW (SPS-2); (b, d) Depositing with the hydrogen flow rate of 6 L/min and spraying power of 20 kW (SPS-3).

that affect the morphology of the coating, since they can influence the melting behavior of the particles. Hou et al. [19] used to report that the feedstock powder was more fully molten at a higher spraying power due to a higher temperature of the plasma jet. Therefore, as the spraying power increases, the temperature of the plasma jet increases, which will improve the melting degree of the in-flight powder, and vice versa. For the auxiliary gas hydrogen, the presence of hydrogen in the plasma can enhance the heat transfer coefficient by increasing the thermal conductivity of the gas, thus the melting degree of the particles can be improved during the spraying [20,21]. It has been reported that the enthalpy input to the gas can be increased by 1.4–2 times by the addition of a small amount of hydrogen [22]. Comparing the coating surface SPS-2 and SPS-1, when the spraying power and the flow rate of hydrogen increased, the nano-structures appeared on the coating surface as the plasma jet temperature increased. The same rule can also be found when comparing the coating surface SPS-2 and SPS-3, the nano-structures appeared on the surface when the heating and melting degree of the particles increased with the increasing of the gas flow rate of hydrogen. In addition, the increase in spraying power was beneficial to the improvement of the coverage density of the nanostructures on the coating surface as can be seen from Figs. 2(b) and 3(b). Based on the above results, increasing the temperature of the particles in the plasma jet facilitated the formation of nanostructures on the coating surface.

3.2. Wettability transition of the coating surface in ambient air

The freshly as-sprayed coating surfaces all exhibited super-hydrophilicity with a water contact angle of 0° in the initial stage after spraying. The droplet infiltrated the surface immediately when dropped on the surface. An interesting phenomenon was observed on the coating surface that the surface wettability can change over time when they stored in ambient air. That is the wettability transition from super-hydrophilicity to hydrophobicity or even super-hydrophobicity can occur on the coating surface without any treatment. This phenomenon was repetitive and has been verified several times. Fig. 4 shows the evolution of water contact angle on the coating surfaces with two typical micro-structures, including micro-nano structured surface (as the surface shown in Fig. 2) and micron structured surface (as the surface shown in Fig. 3(a)), respectively.

As can be seen from Fig. 4, the surface with a micro-nano hierarchical structure can change from super-hydrophilicity to hydrophobicity (contact angle larger than 90°) after storage in air about 30 days. After 60 days, the surface can achieve a super-hydrophobic performance. With the storage time extended, the hydrophobic performance remained essentially unchanged. The contact angle of

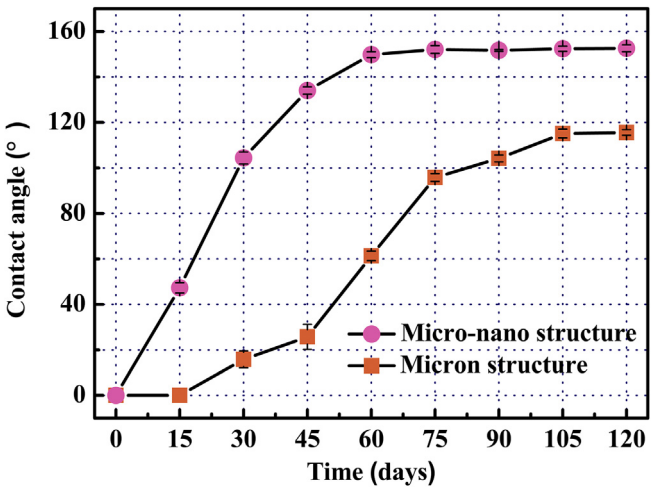

Fig. 4. The evolution of water contact angle of the coating surface with different microstructures in ambient air. The surface with micro-nano hierarchical structures corresponded to the coating SPS-1, and the surface with micron structures corresponded to the coating SPS-2.

the water droplets on the surface was as high as 152.6 ± 1.5° and the sliding angle was as low as 2.0 ± 0.3°. The images of static contact angle of the droplet on the surface and the sliding process of the droplet are shown in Fig. 5(a and b). However, the transition was not very significant on the surface with only micron structures. The surface required at least 75 days to allow the surface to be converted from super-hydrophilicity to hydrophobicity. After about 105 days, the contact angle reached the maximum value, and with the storage time being extended, the hydrophobic performance remained unchanged. The contact angle of the water droplets on the surface was only 115.6 ± 1.2°. Water droplets pinned to the surface and can not slide when the surface was tilted or even rotated with 180°, as the images shown in Fig. 5(c and d).

Under the same storage condition, the degree of change in wettability on coating surfaces was different, indicating that the surface structure had an important effect on the transition process. The wettability transition rate of the surface with nanostructures was higher and a better hydrophobic performance can be obtained on the surface. Therefore, the formation of the nanostructures and the effects of nanostructures on surface wettability will be studied systematically in the following sections.

3.3. Formation of the nanostructures

In this section, a designed shield deposition method was used for surface deposition. The schematic diagram of the setting is presented in Fig. 6. During the deposition process, the separation distance from the shroud exit to the substrate surface was still set as 15 mm. A mirror polished copper was used as the substrate, and a baffle having a width of 40 mm was placed in front of the substrate. The distance between the baffle and the substrate surface was 5 mm. The process parameters were consistent with that used in the preparation of the coating surface of SPS-1.

As can be seen from Fig. 7, the surface formed entirely by pure nanostructures was successfully obtained on the shadowed

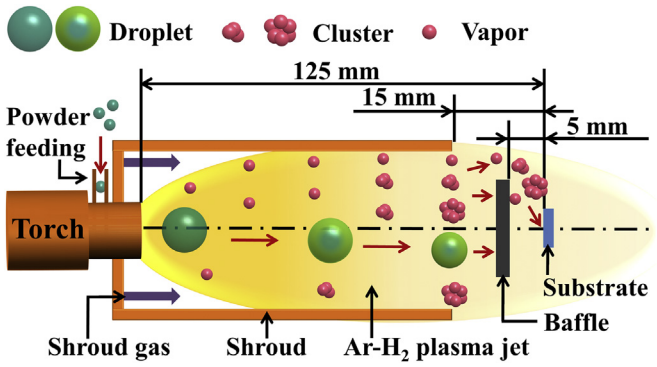

Fig. 6. A schematic diagram of deposition process on a shadowed substrate during the shrouded plasma spraying.

substrate surface. A large number of convex cluster-like structures randomly distributed on the surface were formed by the agglomeration of the nanostructures. The morphology the nanostructures was consistent with that observed on the shrouded plasma sprayed coating surface with fluffy features. The detailed structural information and composition of the nanostructures was characterized by transmission electron microscopy. The result shown in Fig. 8(a) revealed that the nanostructures were composed by a large number of nearly spherical-like particles of less than 100 nm in size. The particle size distribution was not uniform, the size of the larger particles was above 50 nm while the size of the smaller one was below 10 nm. EDX analysis (in Fig. 8(b)) on the nano particles shows the presence of the Ni and Cr element, which demonstrated that the nanostructures obtained by the shield deposition method was derived from Ni20Cr powder.

According to the observation from SEM and TEM, the size of the nanostructures was much smaller than that of the original feedstock particles, so the nanostructures should not be formed from

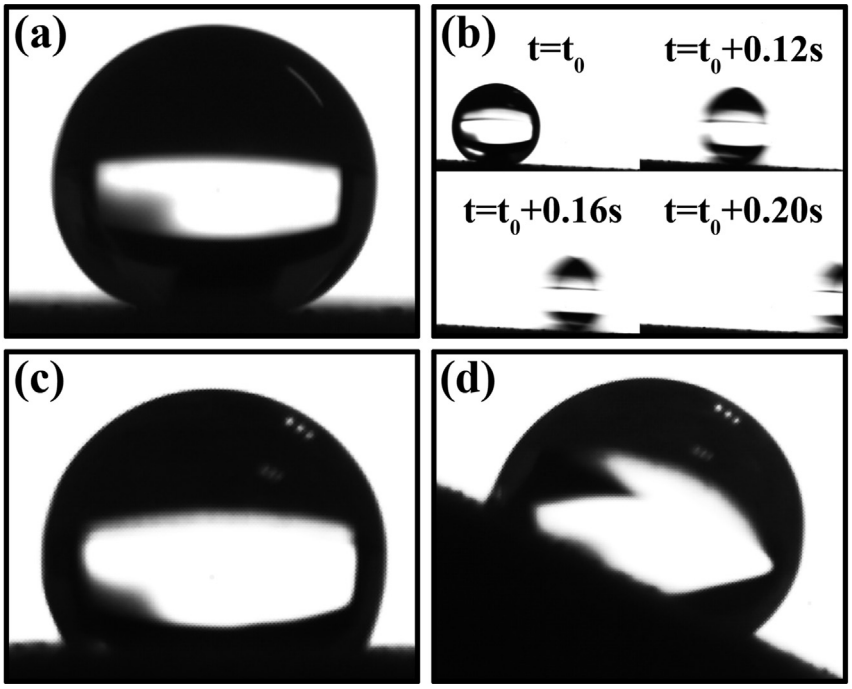

Fig. 5. The optical images of water droplets on the coating surfaces after storage in ambient air for more than 120 days. The coating surface (SPS-1) consisted with micro-nano hierarchical structures with (a) a water contact angle of 152.6° and (b) sliding angle of 2°. The coating surface (SPS-2) consisted with micron structures with (c) a water contact angle of 115.6° and (d) the water droplet pinned to the surface without sliding when the surface was tilted with 25° (the maximum tilt angle of the device).

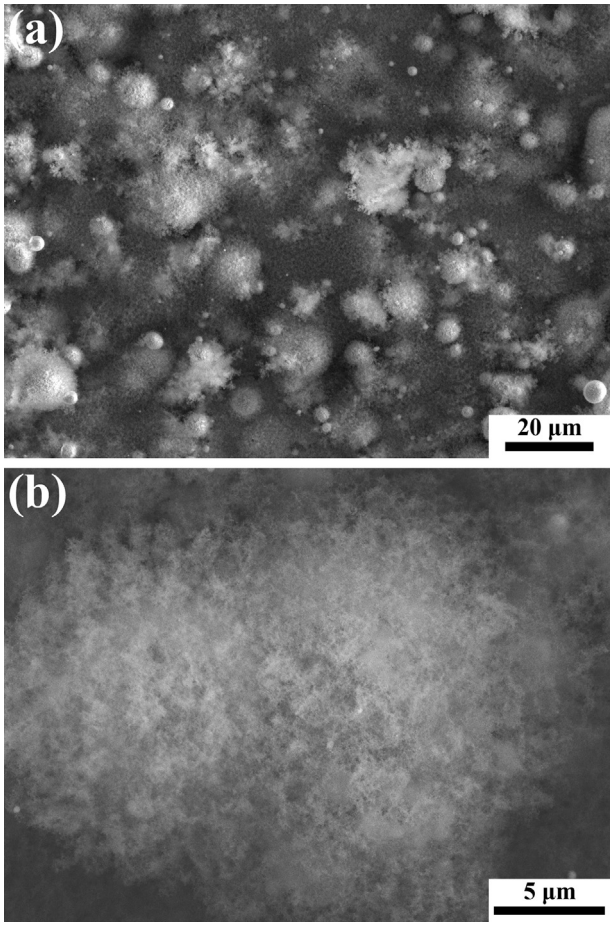

Fig. 7. SEM images of the surface nanostructures formed by shield deposition on the shadowed substrate under different magnification.

liquid deposition of the molten particles with micron size. In atmospheric plasma spraying, the temperature of the plasma jet center is as high as 10000–15000 K. Powder materials are heated during the in-flight stage in the plasma jet. At high temperatures, vaporization of the materials is an inevitable phenomenon, especially for metals and alloys with high thermal conductivity. Vardelle et al. [22,23] used to report the vaporization phenomenon of metallic materials in plasma spraying. Generally, physical vaporization can occur between the free stream and the particle surface at temperatures below the boiling point of the materials [20,22]. During the spraying, molten or semi-molten particles with large size flew in a straight line in the plasma jet due to inertia. When a baffle was placed in front of the substrate, liquid particles cannot be able to pass around the baffle and to deposit on the shadowed substrate, the particles will be filtered out by the baffle. For the vapors with a light quality, due to the plasma jet belongs to turbulence, with the effect of thermal agitation, they can transport in the plasma gas stream. The gas stream was able to flow around complex geometries with high velocity and was forced to go through the shadowed areas. Since vapors transported inside the gas stream, they can deposit on the shadowed substrate. This process had a non-line-of-sight deposition feature [24–26]. Therefore, the nanostructures containing nickel and chromium elements obtained on the shadowed copper substrate should be the products of vapor deposition during the spraying. The nanostructures appeared on the coating surface should also be formed in the same way. Furthermore, the results shown in Section 3.1 indicated that increasing the temperature of the particles in the plasma jet facilitated the formation of nanostructures. This was another strong evidence for the nanostructures came from vapor deposition, since the increase in temperature can promote vaporization of the material and accelerate the process of vapor deposition, which increased the content of nanostructure deposited on the coating surface. The above studies demonstrated the nanostructures appeared on the surface was formed by vapor deposition during the shroud plasma spraying.

The enthalpy of vaporization of metal nickel and chromium is 377.5 and 339.5 $kJ \cdot mol^{-1}$, respectively [27]. Since the difference in the enthalpy of vaporization was small, both nickel and chromium can evaporate at high temperatures and deposit, as shown in the detection result of EDX. Generally, a flat surface structure can be obtained when atoms in vapor phase deposited on a smooth substrate surface. However, the vapor deposited surface in this research presented a rough surface morphology of micro-nano structure (in Fig. 7). This suggests that, in addition to the atoms, clusters were formed by aggregation of the atoms in vapor phase. Atoms and clusters were co-deposited on the substrate surface during the plasma spraying, creating a rough morphology [28]. In the vapor phase, the magnitude of the atomic diameter is about 10^{-10} m, while the cluster is usually composed of several or a dozen atoms [24]. The result of TEM showed that the vapor deposited nanostructures were constructed by the nano particles with the diameter less than 100 nm. These nano particles should be formed

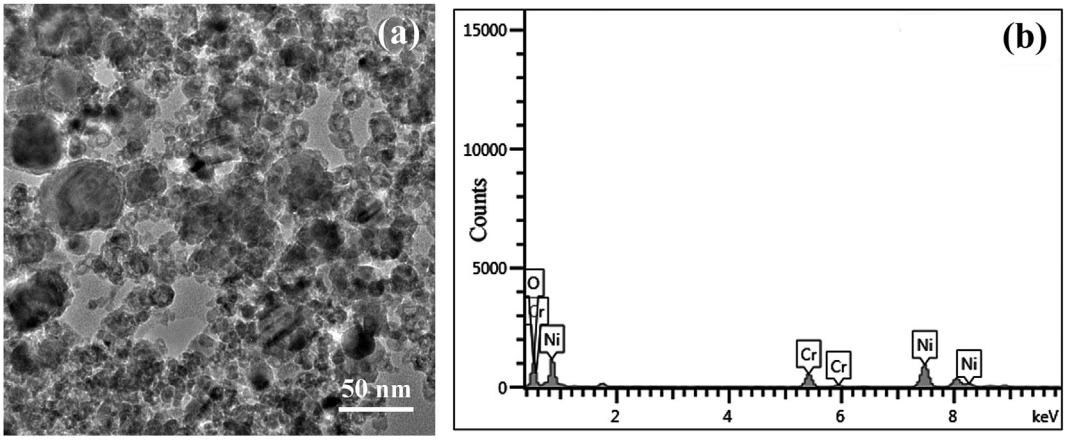

Fig. 8. The results detected by transmission electron microscopy. (a) TEM image of the nano particles which formed the nanostructures. (b) EDX spectrum taken from the nano particles shown in (a).

by the growth of the atoms and clusters.

The substrate temperature has an important effect on vapor deposition. In this research, the average temperature of the substrate was detected as 265 °C during the coating deposition process, which was much lower than the melting point of Ni20Cr, that it favored vapor condensation. Meanwhile, the low substrate temperature as well as the atmospheric environment resulted in a high cooling rate after vapor deposition. It is reported that the estimated cooling rate of the melted particles is in order of 10^6 K/s [23]. High-speed cooling conditions inhibited the growth of grains, thus the fine nano particles were produced. A large number of vapor phases accumulated on the surface continuously, forming the nanostructures with a fluff-like feature.

EDX result showed the presence of the Ni, Cr and O elements on the nano particles. XPS was used to get further detailed information about the nanostructures composition. The high resolution XPS spectra of Ni 2p, Cr 2p and O 1s are shown in Fig. 9. The Ni 2p1/2 and Ni 2p3/2 peaks in Fig. 9(a) at 879.7, 873.8, 861.5 and 855.5 eV can be assigned to NiO. The peaks in Fig. 9(b) at 586.0 and 576.3 eV can be assigned to Cr_2O_3. The existence of metallic nickel and chromium on the surface can be excluded since their characteristic features were not detected. In addition, the O 1s spectrum in Fig. 9(c) was resolved into two peaks at 530.6, and 531.2 eV, corresponding to oxide and hydroxyl, respectively [16]. The above assignments matched very well with the XPS handbook [29]. The results show that the nanostructures were mainly composed of oxides.

During the spraying, the shroud had a great effect on restricting the entrance of the air into the shroud and the non-oxidizing gas argon was used for the protection inside the shroud, the oxidation of the material can be effectively prevented during the in-flight stage inside the shroud. However, due to the high temperature of plasma jet and the large amounts of oxidizing gas presented in ambient air, metallic materials usually accompanied by oxidation even with the shroud protection. When the plasma jet left the shroud exit zone and sprayed into the open air, the air was entrained in the short 15 mm gap between the shroud and the substrate, which can cause the metal to be oxidized. Furthermore, oxidation of the metal vapors can occur during the post-depositional stage when the vapors full contacted with the surrounding air environment before cooling down [30]. Further detailed investigation into the oxidation mechanism is still required in future research.

3.4. Effect of nanostructures on surface wettability

Numerous studies showed that surface chemical composition and geometrical structure are the two crucial factors influencing the wettability of the surface [7]. The effect of nanostructures on surface wettability transition and degree of hydrophobicity will be discussed based on these two factors, respectively.

A Fourier transform infrared spectroscopy (FT-IR) was used to analysis the chemical composition of the pure nanostructures formed by the shield deposition method. Two states of nanostructures were used for the detection, including the freshly as-sprayed state and the state after storage in air for 120 days. Fig. 10 shows the spectra results which were normalized using the peak of the oxide as a standard before contrasting.

As can be seen from the spectrum of the freshly as-sprayed nanostructures, only the peaks representing the oxide and the hydroxyl group appeared, where the peak at 521 cm^{-1} corresponded to the oxide and the peak at 3489 cm^{-1} was the stretching vibration absorption of the O-H [31,32]. This result was consistent with the XPS detection. For the nanostructures after storage in air, in addition to the peaks appeared in the freshly as-sprayed state,

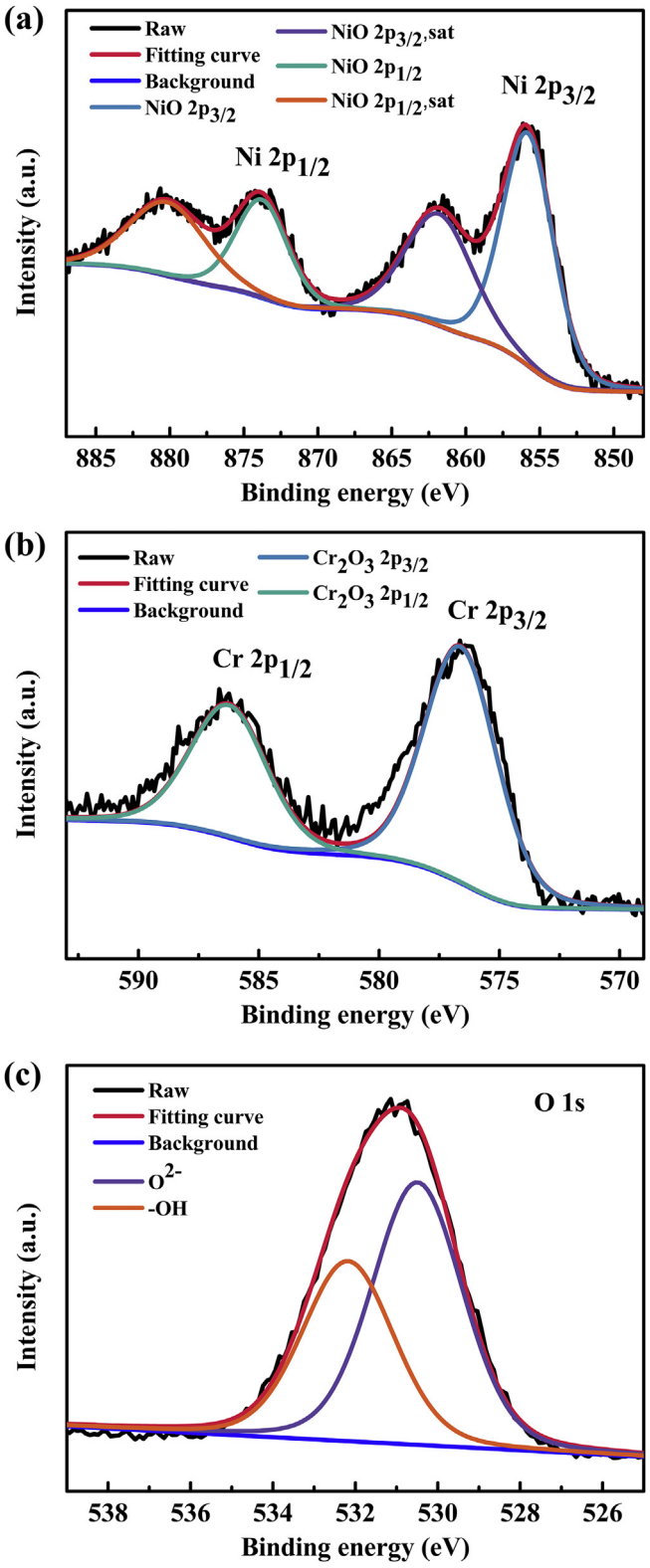

Fig. 9. The XPS result of the nanostructures deposited by the shield deposition method. The high resolution XPS spectra of (a) Ni 2p1/2 and Ni 2p3/2, (b) Cr 2p1/2 and Cr 2p3/2 and (c) O 1s.

the new absorption peaks of hydrocarbons and carboxylates were detected. In the high-frequency region near 3000 cm^{-1}, the peaks at 2927 cm^{-1} and 2856 cm^{-1} were attributed to the asymmetric

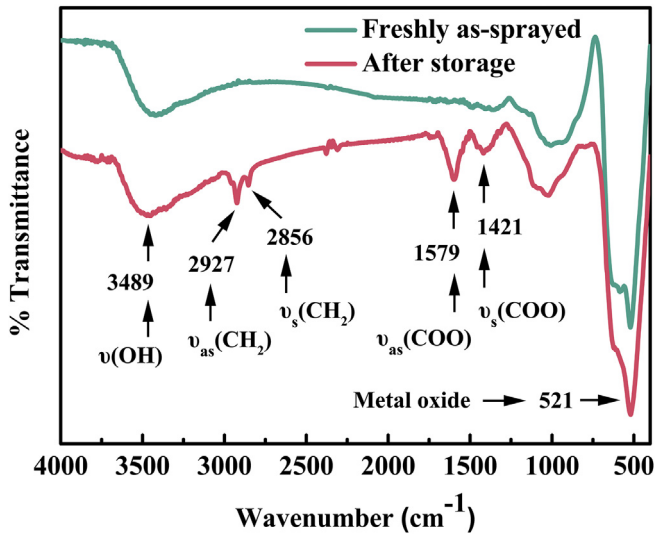

Fig. 10. The FT-IR spectra of the nanostructures at two states, the freshly as-sprayed state and the state after storage in air for more than 120 days.

and symmetric stretching vibrations of the saturated CH_2, respectively [33]. In the low-frequency region, the two peaks detected at 1579 cm^{-1} and 1421 cm^{-1} were ascribed to the asymmetric and symmetric stretching absorptions of the carboxyl (COO), respectively [34]. Since the hydrocarbon was the only detected group in addition to the carboxyl group, saturated hydrocarbon chains should present in the carboxylates. The results of FT-IR showed that the nanostructures were capable of spontaneously adsorbing hydrocarbons and their derivatives during the storage in air.

Metal oxide and the hydroxyl group are hydrophilic, the surface free energy of which is higher than that of water (~72.8 mJ m^{-2} at 295.15 K) [35,36]. TEM image shows that the nanostructures were consisted with a large number of nano particles with the size less than 100 nm, which can lead to the presence of a large number of defects. Thus, the oxide nanostructures had a high surface free energy at the initial stage. Due to the nanostructure surface need to maintain a more stable state, the adsorption of the materials with low surface free energy occurred. It is reported that the hydrocarbon groups are intrinsically hydrophobic, since the surface free energy of the hydrocarbon-only chain is as low as 24 mN/m [37]. Hydrocarbons and their derivatives were reported that exist almost everywhere and their concentration in air is typically parts-perpmillion, so they become the most preferred materials for the adsorption [16,38]. As a result, the adsorption of nanostructures was a spontaneous process and had a selective characteristic in air. The phenomenon of spontaneous adsorbing airborne hydrocarbons on the surface was consistent with some published research [15,16,39].

For the micro-nano hierarchical structured coating surface deposited by vapor-liquid co-deposition, the results of XPS shown in Figs. S1(a and c) in the supplementary material reflected that the nanostructures on the coating surface was composed of NiO and Cr_2O_3, indicating that the vapor deposited nanostructures obtained by the coating deposition process can be considered the same as that obtained by the shield deposition method, although the deposition conditions of them were slightly different. The oxide nanostructures appeared on the top of the coating surface. Changes in the adsorption state of the nanostructures directly lead to the change in the chemical composition of the coating surface. As the surface morphology remained virtually unchanged during the storage, the newly emerging hydrophobic groups on the nanostructures were the main cause of the surface wettability transition. For the micron structured coating surface deposited by liquid deposition, the results of XPS shown in Figs. S1(b and d) in the supplementary material showed that the surface layer was covered by the oxides, including NiO and Cr_2O_3 even with the absence of nanostructures. The rough surface structure indicated that defects were inevitably present on the surface. This means that the surface also required and had the ability to adsorb hydrocarbons and their derivatives to reduce its surface free energy. Thus, the surface wettability can change as shown in Fig. 4.

The amount of low surface free energy adsorbates had an important effect on the hydrophobicity of the coating surface. As can be seen from Fig. 4, when the two coatings after storage in air for a certain period of time, the contact angle of water droplets on both of the surfaces no longer changed with the extension of the storage time, the hydrophobicity tended to be stable. This phenomenon indicated that the content of surface adsorbates reached saturation.

XPS was used to detect the two coating surfaces where the adsorption reached a saturated state, and the results are shown in Fig. 11. The decomposition of the high-resolution C 1s peak was performed to analyze the state and relative content of carbon-containing adsorbates on the surface. Fig. 11(c and d) represent the deconvoluted spectra from the C 1s, which were resolved into three contributions with binding energies of 284.6, 286.3, and 288.6 eV, corresponding to C-C/C-H, C-O, and COO^-, respectively [40]. C−C/C−H was corresponded to the hydrocarbon groups detected in the infrared spectrum. By calculating the area occupied by the spectral peak in the deconvoluted spectra, the relative content of C−C/C−H was 85.8% on the micro-nano hierarchical structured surface (Fig. 11(c)) and was 87.3% on the micron structured surface (Fig. 11(d)), respectively. The results indicated that the content of hydrocarbons and their derivatives were predominant in carbonaceous substances on the both coating surfaces. Based on the above analysis, the C atomic content relative to the metal (nickel and chromium) atomic content, represented by the atomic ratio C/M, can be used to evaluate the relative content of hydrocarbon adsorbates on the coating surface. By calculating the results of element content listed in Fig. 11(a and b), the ratio of C/M on the micro-nano structured surface was 2.55, the value of which was larger than the value 1.48 on the micron structured surface. The result indicated that the content of adsorbed hydrocarbons on the coating surface which had the vapor deposited nanostructures was relatively higher. As a result, a high content of low surface free energy adsorbates was one of the reasons that the hydrophobicity of the micro-nano hierarchical structured coating surface was better than that of the micron structured surface.

As can be seen from Fig. 4, the time required for the wettability transition of the nano structured surface was significantly less than that of the micron structured surface, which indicated that the adsorption rate of the nanostructures was faster than the micron structure. Comparing with the relatively flat micron structures, the nanostructures may have more defects, resulting in a higher surface free energy. In addition, the nanostructures have a large specific surface area. It can be speculated that the adsorption capacity of the nanostructures should be stronger than that of the micron structure. Boinovich et al. [39] have reported that the spontaneous adsorb of hydrocarbon molecules on rough surfaces was more intensive than on flat surfaces. Therefore, the adsorption rate of the nanostructures was fast and the content of hydrocarbons adsorbed by nanostructures was high.

In addition, surface structure was also the key to affect surface hydrophobicity when the surface has low surface free energy. The theoretical calculations showed that, on the smooth surface, even with the lowest surface free energy, the contact angle of the droplet

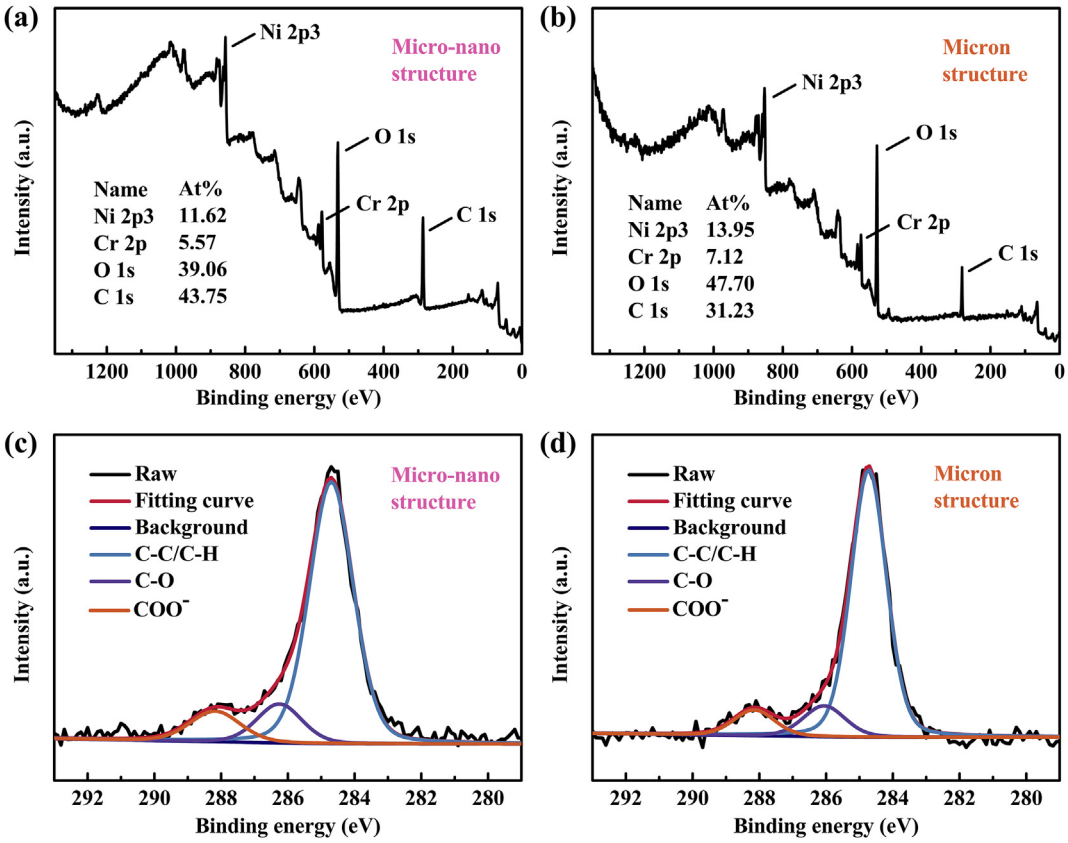

Fig. 11. The XPS survey spectra and the deconvolution of the high-resolution C 1s. (a, c) The surface presented micro-nano structures, and (b, d) the surface presented micron structures. The data inserted in Fig. (a) and (b) are the element contents on the coating surface. The coatings have been stored in air for more than 120 days.

cannot greater than 120° [41]. Based on Cassie-Baxter's theory, when the droplet is in contact with the surface, the composite solid-liquid-gas interface is formed as the air can be trapped inside the cavities formed by the rough structure. According to the theory, reducing the value of solid-liquid contact fraction is the key point to improving the surface hydrophobicity [10]. Fig. 12 shows the schematic representation of the two typical shrouded plasma sprayed coating surfaces in contact with water droplets. For the

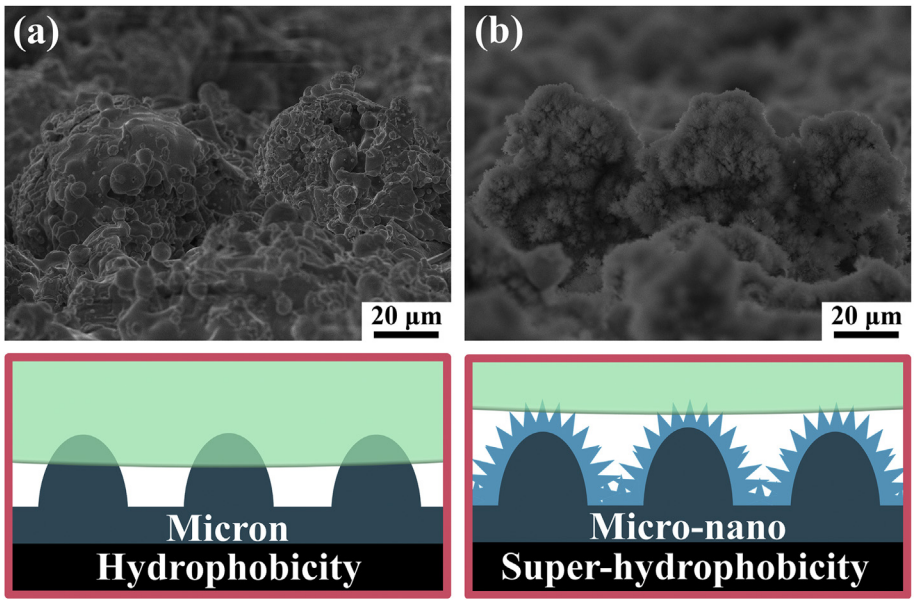

Fig. 12. SEM images of the coating surfaces with different structural features include (a) micron structure deposited by the liquid phase, and (b) micro-nano hierarchical structure formed by vapor-liquid co-deposition. The corresponding images below are the models of solid-liquid interface between the water and the surface.

surface formed by micron structures as shown in Fig. 12(a), air can be trapped between the micron structures. Due to the spacing between the micron structures, the water droplet will form a certain depression on the surface under the action of gravity. With a large contact area between the droplet and the surface, the surface only exhibited hydrophobic property and the droplet was easily pinned to the surface. When the nanostructures constructed by vapor deposition on the surface, in addition to the air cushion formed by the micron structures, the fluffy nanostructures at the top of the surface can maintain more cavitation to prevent droplet contact with the surface. As the schematic diagram shown in Fig. 12(b), the surface has more hydrophobic and less adhesive state compared to the surface shown in Fig. 12(a). Feng et al. [42] used to point out that high contact angle can be induced by nanostructures and low sliding angle can be achieved by constructing micro-nano structures, since a large amount of air can be trapped between the droplet and the surface. Therefore, the typical micro-nano hierarchical structure deposited by vapor-liquid co-deposition was conducive to obtain super-hydrophobic property of the surface.

Through the study of chemical composition and structure, it was found that nanostructures have a selective spontaneous adsorption characteristic to reduce the surface free energy, and their deposition on the coating surface can effectively reduce the contact area between the droplet and the surface. These two factors together affected the wettability of the coating surface. Therefore, the formation of nanostructures by vapor deposition was of great importance for obtaining super-hydrophobicity on the surface.

4. Conclusions

In this paper, we developed and systematically studied the method of constructing nanostructures on the coating surface by controlling the vapor deposition during shrouded plasma spraying of Ni20Cr coating. The increase of heating degree of the particles in the spraying was favorable for the deposition of nanostructures. It was demonstrated that the morphology of vapor phase deposition on the surface showed nanostructures, which had fluff-like features formed by the agglomeration of nano particles with sizes less than 100 nm. The nanostructures were composed of metal oxides, including NiO and Cr_2O_3. A large number of defects and a large specific surface area make the nanostructures have a stronger ability to selectively adsorb low surface free energy hy-dro-carbons and their de-riv-a-tives in air than the micron structures. Meanwhile, the nanostructures distributed on the top of the micron structures can provide more air cushion to prevent droplet contact with the surface. Therefore, without any chemical modification, the coating surface with a unique micro-nano hierarchical structure formed by vapor-liquid co-deposition can change from super-hydrophilicity to super-hydrophobicity with a water contact angle of 152.6 ± 1.5° and sliding angle of 2.0 ± 0.3° when stored in air.

Funding

This work was supported by the National Basic Research Program of China [2012CB625100].

Contributors

Jie Li conducted the experiments with assistance from Chengxin Li, Guanjun Yang and Changjiu Li. Chengxin Li provided supervision of all experimental work and writing. The manuscript was written through the contributions of all authors. All authors have given approval to the final version of the manuscript. The authors declare no competing financial interest.

Acknowledgments

The authors acknowledged the funding support from the National Basic Research Program of China [2012CB625100].

Appendix A. Supplementary data

Supplementary data related to this article can be found at https://doi.org/10.1016/j.jallcom.2017.11.135.

References

[1] Z. Zeng, S. Kuroda, J. Kawakita, M. Komatsu, H. Era, Effects of some light alloying elements on the oxidation behavior of Fe and Ni-Cr based alloys during air plasma spraying, J. Therm. Spray Technol. 19 (2010) 128–136.
[2] Y.P. Wan, V. Prasad, G.X. Wang, S. Sampath, J.R. Fincke, Model and powder particle heating, melting, resolidification, and evaporation in plasma spraying processes, J. Heat Transf-T ASME 121 (1999) 691–699.
[3] N. Sharifi, M. Pugh, C. Moreau, A. Dolatabadi, Developing hydrophobic and superhydrophobic TiO_2 coatings by plasma spraying, Surf. Coating. Technol. 289 (2016) 29–36.
[4] X. Chen, Y. Gong, X. Suo, J. Huang, Y. Liu, H. Li, Construction of mechanically durable superhydrophobic surfaces by thermal spray deposition and further surface modification, Appl. Surf. Sci. 356 (2015) 639–644.
[5] Z. Li, Y. Zheng, J. Zhao, L. Cui, Wettability of atmospheric plasma sprayed Fe, Ni, Cr and their mixture coatings, J. Therm. Spray Technol. 21 (2012) 255–262.
[6] Z. Li, Y. Zheng, L. Cui, Preparation of metallic coatings with reversibly switchable wettability based on plasma spraying technology, J. Coating Technol. Res. 9 (2012) 579–587.
[7] J.M. Lim, G.R. Yi, J.H. Moon, C.J. Heo, S.M. Yang, Superhydrophobic films of electrospun fibers with multiple-scale surface morphology, Langmuir 23 (2007) 7981–7989.
[8] C. Neinhuis, W. Barthlott, Characterization and distribution of water-repellent, self-cleaning plant surfaces, Ann. Bot-London 79 (1997) 667–677.
[9] X. Zhang, F. Shi, J. Niu, Y. Jiang, Z. Wang, Superhydrophobic surfaces: from structural control to functional application, J. Mater. Chem. 18 (2008) 621–633.
[10] B. Bhushan, Y.C. Jung, Natural and biomimetic artificial surfaces for superhydrophobicity, self-cleaning, low adhesion, and drag reduction, Mater. Sci. 56 (2011) 1–108.
[11] C. Barbe, J. Bartlett, L. Kong, K. Finnie, H.Q. Lin, M. Larkin, S. Calleja, A. Bush, G. Calleja, Silica particle: a novel drug-delivery system, Adv. Mater. 16 (2004) 1959–1966.
[12] T. Hang, A. Hu, H. Ling, M. Li, D. Mao, Super-hydrophobic nickel films with micro-nano hierarchical structure prepared by electrodeposition, Appl. Surf. Sci. 256 (2010) 2400–2404.
[13] F. Tian, A. Hu, M. Li, D. Mao, Superhydrophobic nickel films fabricated by electro and electroless deposition, Appl. Surf. Sci. 258 (2012) 3643–3646.
[14] K. Meng, Y. Jiang, Z. Jiang, J. Lian, Q. Jiang, Cu surfaces with controlled structures: from intrinsically hydrophilic to apparently superhydrophobic, Appl. Surf. Sci. 290 (2014) 320–326.
[15] S. Khorsand, K. Raeissi, F. Ashrafizadeh, M.A. Arenas, Super-hydrophobic nickel-cobalt alloy coating with micro-nano flower-like structure, Chem. Eng. J. 273 (2015) 638–646.
[16] P. Liu, L. Cao, W. Zhao, Y. Xia, W. Huang, Z. Li, Insights into the superhydrophobicity of metallic surfaces prepared by electrodeposition involving spontaneous adsorption of airborne hydrocarbons, Appl. Surf. Sci. 324 (2015) 576–583.
[17] G. Wang, T.Y. Zhang, Oxygen adsorption induced superhydrophilic-to-superhydrophobic transition on hierarchical nanostructured CuO surface, J. Colloid Interface Sci. 377 (2012) 438–441.
[18] A.Y. Vorobyev, C. Guo, Multifunctional surfaces produced by femtosecond laser pulses, J. Appl. Phys. 117 (2015), 033103.
[19] G. Hou, Y. An, G. Liu, H. Zhou, J. Chen, Z. Chen, Effect of atmospheric plasma spraying power on microstructure and properties of WC-$(W,Cr)_2C$-Ni coatings, J. Therm. Spray Technol. 20 (2011) 1150–1160.
[20] Y.P. Wan, J.R. Fincke, S. Sampath, V. Prasad, H. Herman, Modeling and experimental observation of evaporation from oxidizing molybdenum particles entrained in a thermal plasma jet, Int. J. Heat Mass Tran. 45 (2002) 1007–1015.
[21] M. Vardelle, C. Trassy, A. Vardelle, P. Fauchais, Experimental investigation of powder vaporization in thermal plasma jets, Plasma Chem. Plasma Process. 11 (1991) 185–201.
[22] A. Vardelle, M. Vardelle, H. Zhang, N.J. Themelis, K. Gross, Volatilization of metal powders in plasma sprays, J. Therm. Spray Technol. 11 (2002) 244–252.
[23] M. Vardelle, A. Vardelle, K.I. Li, P. Fauchais, Coating generation: vaporization of particles in plasma spraying and splat formation, Pure Appl. Chem. 68 (1996) 1093–1099.
[24] Q.Y. Chen, C.X. Li, T. Wei, H.B. Sun, S.L. Zhang, X.T. Luo, G.J. Yang, C.J. Li, M.L. Liu, Controlling grain size in columnar YSZ coating formation by droplet filtering assisted PS-PVD processing, RSC Adv 5 (2015) 102126–102133.

[25] L. Zhu, N. Zhang, R. Bolot, M.P. Planche, H. Liao, C. Coddet, Very low pressure plasma sprayed yttria-stabilized zirconia coating using a low-energy plasma gun, Appl. Phys. A 105 (2011) 991–996.
[26] K. von Niessen, M. Gindrat, Plasma spray-PVD: a new thermal spray process to deposit out of the vapor phase, J. Therm. Spray Technol. 20 (2011) 736–743.
[27] J.G. Speight, Lange's Handbook of Chemistry, sixteenth ed., McGraw-Hill, New York, 2005.
[28] Q.Y. Chen, C.X. Li, J.Z. Zhao, G.J. Yang, C.J. Li, Microstructure of YSZ coatings deposited by PS-PVD using 45 kW shrouded plasma torch, Mater. Manuf. Process. 31 (2015) 1183–1191.
[29] C.D. Wagner, W.M. Riggs, L.E. Davis, J.F. Moulder, G.E. Muilenberg, Handbook of X-ray Photoelectron Spectroscopy, Perkin-Elmer Corp, Eden Prairie, 1979.
[30] S. Matthews, Shrouded plasma spray of Ni-20Cr coatings utilizing internal shroud film cooling, Surf. Coating. Technol. 249 (2014) 56–74.
[31] X. Chen, J. Yuan, J. Huang, K. Ren, Y. Liu, S. Lu, H. Li, Large-scale fabrication of superhydrophobic polyurethane/nano-Al_2O_3 coatings by suspension flame spraying for anti-corrosion applications, Appl. Surf. Sci. 311 (2014) 864–869.
[32] G. Verma, S.K. Dhoke, A.S. Khanna, Polyester based-siloxane modified waterborne anticorrosive hydrophobic coating on copper, Surf. Coating. Technol. 212 (2012) 101–108.
[33] S.H. Lee, Z.R. Dilworth, E. Hsiao, A.L. Barnette, M. Marino, J.H. Kim, J.G. Kang, T.H. Jung, S.H. Kim, One-step production of superhydrophobic coatings on flat substrates via atmospheric Rf plasma process using non-fluorinated hydrocarbons, ACS Appl. Mater. Inter 3 (2011) 476–481.
[34] S. Alexander, J. Eastoe, A.M. Lord, F. Guittard, A.R. Barron, Branched hydrocarbon low surface energy materials for superhydrophobic nanoparticle derived surfaces, ACS Appl. Mater. Inter 8 (2016) 660–666.
[35] S. Takeda, M. Fukawa, Y. Hayashi, K. Matsumoto, Surface OH group governing adsorption properties of metal oxide films, Thin Solid Films 339 (1999) 220–224.
[36] J. Drelich, E. Chibowski, D.D. Meng, K. Terpilowski, Hydrophilic and superhydrophilic surfaces and materials, Soft Matter 7 (2011) 9804–9828.
[37] M. Sagisaka, T. Narumi, M. Niwase, S. Narita, A. Ohata, C. James, A. Yoshizawa, E.T. de Givenchy, F. Guittard, S. Alexander, J. Eastoe, Hyperbranched hydrocarbon surfactants give fluorocarbon-like low surface energies, Langmuir 30 (2014) 6057–6063.
[38] D.B. Millet, N.M. Donahue, S.N. Pandis, A. Polidori, C.O. Stanier, B.J. Turpin, A.H. Goldstein, Atmospheric volatile organic compound measurements during the Pittsburgh Air Quality Study: results, interpretation, and quantification of primary and secondary contributions, J. Geophys. Res. 110 (2005), D07S07.
[39] L.B. Boinovich, A.M. Emelyanenko, A.S. Pashinin, C.H. Lee, J. Drelich, Y.K. Yap, Origins of thermodynamically stable superhydrophobicity of boron nitride nanotubes coatings, Langmuir 28 (2012) 1206–1216.
[40] J. Long, M. Zhong, H. Zhang, P. Fan, Superhydrophilicity to superhydrophobicity transition of picosecond laser microstructured aluminum in ambient air, J. Colloid Interface Sci. 441 (2015) 1–9.
[41] W. Barthlott, C. Neinhuis, Purity of the sacred lotus, or escape from contamination in biological surfaces, Planta 202 (1997) 1–8.
[42] L. Feng, S. Li, Y. Li, H. Li, L. Zhang, Y. Song, B. Liu, L. Jiang, D. Zhu, Super-hydrophobic surfaces: from natural to artificial, Adv. Mater. 14 (2002) 1857–1860.